The Mn, Mg-intracrystalline exchange reaction in donpeacorite ($Mn_{0.54}Ca_{0.03}Mg_{1.43}Si_2O_6$) and its relation to the fractionation behavior of Mn in Fe, Mg-orthopyroxene

MARILENA STIMPFL*

University of Arizona, Lunar and Planetary Laboratory, Tucson, Arizona 85721, U.S.A.

ABSTRACT

The equilibrium intracrystalline distribution of Mn and Mg between the M1 and M2 sites of a Mn-rich/Fe-free orthopyroxene (donpeacorite) was investigated by means of annealing experiments at temperatures between 980 and 800 °C and single-crystal X-ray diffraction. The data show that Mn, as does Fe^{2+} in Fe-Mg orthopyroxene, preferentially orders at the M2 site. However, comparison of the distribution coefficient $k_{D(Mn-Mg)}$ determined in this study with k_{D*} measured for Fe-Mg orthopyroxene shows that Mn has a much stronger preference for the M2 site relative to Fe^{2+}. This result implies that the practice to partition $Fe^{2+} + Mn = Fe^*$ as one species, typically implemented to determine the quenched-site occupancies in Fe-rich/Mn-poor orthopyroxene, should be abandoned and that Mn should be considered totally ordered at M2. The partitioning method, i.e., Fe vs. Fe*, has implications for the determination of cooling rates from the observed ordering state of orthopyroxene, particularly for Fe-poor compositions (Fs < 0.16).

INTRODUCTION

The fractionation of cations over different crystallographic sites, also known as order/disorder (O/D) or intracrystalline exchange reaction, has been extensively studied in orthopyroxene due to its potential to provide insights into the temperature-time (*T*-t) history of the host rock (e.g., Ganguly et al. 1994; Ganguly and Domeneghetti 1996; Ganguly and Stimpfl 2000; Heinemann et al. 2000; Kroll et al. 1997; Zema et al. 1997). The reaction has been well characterized in Fe-Mg pyroxenes (e.g., Anovitz et al. 1988; Besancon 1981; Ganguly and Tazzoli 1994; Molin et al. 1991; Stimpfl et al. 1999; and references therein) but no systematic study has been published on the partitioning behavior of Mn. In fact, Mn is often treated as equivalent to Fe^{2+} and the two elements are combined as the fictive species $Fe^* = Fe^{2+} + Mn$ (e.g., Ganguly and Domeneghetti 1996; Ganguly et al. 1994; Stimpfl and Ganguly 2002; Zema et al. 1997; and references therein).

Understanding the partitioning behavior of Mn in Fe-Mg orthopyroxene might appear to be a marginal issue because the concentration of Mn in natural Fe^{2+}-Mg orthopyroxene is usually very low (MnO < 1%). However, usage of the O/D reaction to unravel the thermal history of rocks requires that the site occupancies be known with the highest precision possible to permit a reliable retrieval of cooling rates.

Partitioning of Fe* was rationalized by Hawthorne and Ito (1978) who refined the structure of a synthetic Mn-rich orthopyroxene [$(Mg_{0.925}Mn_{0.075})SiO_3$] and reported that Mn fractionated over both octahedral sites (M1 and M2), preferentially ordering at M2. On the other hand, Petersen et al. (1984) noted in the naturally occurring Mn-rich/Fe-free orthopyroxene (donpeacorite),

that Mn was totally ordered at M2. This configuration could be the result of either the *T*-t history of the sample (slow cooling would favor ordered states) or to an absence of intracrystalline fractionation of Mn, in contrast to the observation of Hawthorne and Ito (1978). Both studies show that the ordering trend of Mn is the same as that of Fe^{2+} in Fe-Mg orthopyroxene, but it remains to be demonstrated that both Mn and Fe^{2+} display the same degree of preference for the M2 site.

This work aims to determine the equilibrium intracrystalline distribution of Mn and Mg between the M1 and M2 sites in donpeacorite as a function of temperature. The results will test if Mn and Fe^{2+} have the same preference for the M2 site, and therefore, if the assumption underlying the partitioning of Fe* in Fe-Mg orthopyroxene is justified.

EXPERIMENTAL METHODS

The Mn-rich orthopyroxene used in this work occurs in Mn-rich siliceous marbles which are distributed within several siliceous marble units at Balmat, N.Y. (Petersen et al. 1984). These marbles, common throughout the Adirondack Lowlands, were metamorphosed to the upper amphibolite facies during the 1.0 Ga Grenville Orogeny.

A series of annealing experiments were conducted using a donpeacorite crystal ($0.4 \times 0.3 \times 0.2$ mm) to determine the equilibrium fractionation for the O/D reaction. Single-crystal X-ray intensity data for the crystal (DP1) were collected prior to thermal annealing to determine the original site occupancy distribution, and then after each annealing experiment. Site occupancies were determined by means of X-ray diffraction (XRD) and structural refinement using bulk chemical constraints. The chemical composition for the crystal used in this work was determined from electron microprobe data after all the experiments were completed.

Heating experiments

The equilibrium fractionation of DP1 was constrained by means of both ordering and disordering experiments. The sample was disordered successively at several temperatures up to 980 °C and then was ordered at several temperatures down to 806 °C. The crystal was annealed at a particular temperature until a steady state, as determined by time-series study, was achieved. In addition, the equilibrium ordering

* E-mail: mstimpfl@lpl.arizona.edu

state at 900 °C was "reversed"; that is, equilibrium was achieved by approaching it from states which were more ordered (disordering run) and less ordered (ordering run) than the equilibrium state at 900 °C.

All annealing experiments were carried out by sealing DP1, along with a fO_2 buffer mixture of wüstite and iron, in a silica glass tube. The buffer mixture was placed within an Au capsule which was open at one end. The assembly was then suspended at the "hot spot" of a vertical tube furnace. At the end of each experiment the sample was drop-quenched in water. For all runs a Pt-Pt10%Rh thermocouple placed at the side of the charge monitored the temperature. The temperature for all runs was maintained between ±3 °C of the desired temperature.

X-ray data collection

After each annealing experiment, single-crystal X-ray diffraction intensities were recorded with a Bruker SMART1000 (Bruker 1997b) diffractometer equipped with a CCD area detector, using graphite-monochromatized MoKα radiation (λ = 0.71073 Å) from 0° to a maximum of 86° in 2θ (Table 1). A total of 4948 frames was collected for each data set, with each frame consisting of an ω scan of 0.15° width and an X-ray exposure time of 10 s. Data were collected in multirun mode:

six runs were selected to maximize randomness. Of these, 2 short runs of 50 frames were used to monitor the decay of X-ray intensity. After completion of the data collection, the Bruker SAINT software (Bruker 1997a) was used to integrate the observed intensities. The sharpness of the peaks allowed the use of box optimization and narrow frame algorithm as integration conditions; for all the runs the results of the box optimization algorithm converged. The orientation matrix was updated with a frequency of 303 frames to adjust for possible crystal translations, although none were detected. In addition, crystallographic constraints were not imposed on the orientation matrix. Lorentz and polarization corrections were also applied using the program SAINT in the SMART CCD package. Table 1 lists relevant data collection parameters for each experiment.

A total of ~21 000 reflections were recorded for the 980 °C DIS experiment, while for other data collections, between ~ 15 000 and 12 000 reflections were observed. The reflections were integrated in the space group *Pbca* and were corrected for λ/2 factor and absorption using the SADABS program (Sheldrick 1996). Merging and averaging of the equivalent reflections were performed in the Laue point group *mmm* using the SORTAV program (Blessing 1987). A total of ~2200 to ~3000 independent reflections remained after merging (Table 1). Lastly, unit-cell parameters constrained to orthorhombic symmetry were refined using the Bruker SAINT software (Bruker 1997a) and are given in Table 2 for the untreated and the heat-treated sample.

Few reflections violating the *Pbca* extinction conditions were observed for DP1. These exceptions are represented by reflections with indices 0*kl* with *k* = 2*n* + 1 and *l* = 4*n* + 2 observed for the natural sample (0*kl* = 016), for the 900 °C-DIS experiment (0*kl* = 012), and for the 856 °C-ORD experiment (0*kl* = 052). Similar forbidden reflections in Fe-Mg orthopyroxene were observed by Domeneghetti et al. (1995), who concluded that these reflections were consistent with an exsolved *C*2/*c* augitic phase. Because we used the same sample for all the data collections, the crystal changed orientation each time it was mounted on the diffractometer. The fact that the "forbidden reflections" changed indices or were not always observed supports the conclusion that they are due to multiple diffractions rather than to the presence of an exsolved phase within the matrix of the orthopyroxene. In addition, Petersen et al. (1984) did not report any exsolution lamellae in the donpeacorite samples from the same location, which they studied by means of precession and Weissenberg photographs.

TABLE 1. Data collection parameters and integration statistics for the untreated and heat treated DP1 sample

Heat treatment	Untreated	980 °C DIS	900 °C DIS	904 °C ORD	856 °C ORD	806 °C ORD
Max sinθ/λ (Å⁻¹)	0.90	0.96	0.90	0.95	0.92	0.96
Observed 2θ$_{max}$ (°)	79.76	86.47	79.46	85.46	81.6	85.74
CCD distance from crystal (mm)	5.35	3.79	5.35	4.80	5.38	4.80
2θ section covered (°)	52	66	52	56	54	56
No. reflex. measured	12727	20982	12686	14043	12814	15535
Highest redundancy	7.25	9.32	7.62	6.2	7.01	7.49
Lowest redundancy	4.55	5.92	5.08	4.22	4.47	4.61
Unique reflections	2449	3091	2214	2915	2511	2944

Notes: No. reflex. = Number of reflections measured. Abbreviations: DIS = disordering experiments; ORD = ordering experiments).

TABLE 2. Cell parameters and interatomic distances in angstroms for DP1 for the untreated and heat treated sample

Heating treatment	Untreated		980 °C DIS		900 °C DIS		904 °C ORD		856 °C ORD		806 °C ORD	
a	18.3668	(3)	18.3653	(4)	18.3686	(3)	18.3718	(4)	18.3645	(3)	18.3559	(4)
b	8.8725	(2)	8.8819	(3)	8.8828	(2)	8.8836	(2)	8.8810	(2)	8.8741	(2)
c	5.2289	(1)	5.2305	(2)	5.2287	(1)	5.2334	(1)	5.2284	(1)	5.2256	(1)
V	852.10	(5)	853.20	(6)	853.13	(4)	854.01	(5)	852.71	(4)	854.21	(5)
M1 -												
O2A	2.023	(1)	2.027	(1)	2.028	(1)	2.027	(1)	2.026	(1)	2.025	(1)
O1A	2.040	(1)	2.045	(1)	2.044	(1)	2.045	(1)	2.044	(1)	2.043	(1)
O2B	2.047	(1)	2.052	(1)	2.052	(1)	2.051	(1)	2.051	(1)	2.048	(1)
O1B	2.066	(1)	2.072	(1)	2.070	(1)	2.073	(1)	2.069	(1)	2.068	(1)
O1A'	2.146	(1)	2.153	(1)	2.153	(1)	2.154	(1)	2.150	(1)	2.150	(1)
O1B'	2.179	(1)	2.185	(1)	2.184	(1)	2.184	(1)	2.183	(1)	2.181	(1)
<M1-O>	2.084		2.089		2.089		2.089		2.087		2.086	
M2 -												
O2B	2.040	(1)	2.032	(1)	2.032	(1)	2.036	(1)	2.033	(1)	2.033	(1)
O2A	2.109	(1)	2.099	(1)	2.100	(1)	2.101	(1)	2.101	(1)	2.101	(1)
O1B	2.130	(1)	2.123	(1)	2.123	(1)	2.123	(1)	2.123	(1)	2.124	(1)
O1A	2.159	(1)	2.154	(1)	2.153	(1)	2.154	(1)	2.155	(1)	2.152	(1)
O3A	2.329	(1)	2.329	(1)	2.330	(1)	2.329	(1)	2.331	(1)	2.328	(1)
O3B	2.532	(1)	2.536	(1)	2.538	(1)	2.540	(1)	2.536	(1)	2.536	(1)
<M2-O>	2.217		2.212		2.213		2.214		2.213		2.212	
SiA -												
O2A	1.594	(1)	1.593	(1)	1.593	(1)	1.594	(1)	1.593	(1)	1.591	(1)
O1A	1.613	(1)	1.612	(1)	1.612	(1)	1.612	(1)	1.613	(1)	1.612	(1)
O3A	1.646	(1)	1.648	(1)	1.646	(1)	1.648	(1)	1.646	(1)	1.645	(1)
O3A'	1.665	(1)	1.665	(1)	1.666	(1)	1.666	(1)	1.664	(1)	1.663	(1)
SiA-br	1.656		1.657		1.656		1.657		1.655		1.654	
SiA-nbr	1.604		1.603		1.603		1.603		1.603		1.602	
<SiA-O>	1.630		1.630		1.629		1.630		1.629		1.628	
SiB-												
O2B	1.592	(1)	1.591	(1)	1.592	(1)	1.591	(1)	1.590	(1)	1.591	(1)
O1B	1.618	(1)	1.618	(1)	1.619	(1)	1.619	(1)	1.620	(1)	1.619	(1)
O3B	1.668	(1)	1.669	(1)	1.669	(1)	1.669	(1)	1.670	(1)	1.666	(1)
O3B'	1.675	(1)	1.675	(1)	1.674	(1)	1.675	(1)	1.672	(1)	1.673	(1)
SiB-br	1.672		1.672		1.672		1.672		1.671		1.668	
SiB-nbr	1.605		1.605		1.606		1.605		1.605		1.605	
<SiB-O>	1.638		1.638		1.639		1.639		1.638		1.637	

Notes: Standard deviations are given in parenthesis; abbreviations as in Table 1. Space group: P*bca*.

Microprobe analyses

The chemical composition of DP1 was determined from a large number of spot analyses obtained with a CAMECA SX50 electron microprobe (EMP) with a wavelength-dispersive spectrometer (WDS) system using 15 kV accelerating voltage, 20 nA beam current, and counting times of 30 s on the peak and on the background. Each spot was analyzed for Si, Ca, Ti, Cr, Al, Mn, Na, Mg, and Fe, using the following standards: synthetic diopside for Si and Ca; ilmenite for Ti; synthetic chromite for Cr; synthetic pyrope for Al; synthetic spessartine for Mn; natural albite for Na; synthetic enstatite for Mg; and synthetic ferrosilite for Fe.

The orthopyroxene crystal was found to be homogeneous within the analytical resolution of the microprobe (Table 3). The average composition of DP1 along with its respective standard deviations was used to determine its statistically most-probable bulk composition. This was achieved by projecting the average composition of each element, weighted by its respective standard error, on the n-dimensional surface that satisfies the crystal chemical constraints for orthopyroxene (Dollase and Newman 1984; Stimpfl et al. 1999). Usually, the adjusted composition for each element was within ± 1 standard deviation ($\pm\sigma$) of its average composition. The average and adjusted compositions of DP1 are summarized in Table 3.

Site occupancy determination

The site occupancies were refined using the RFINE90 program (Finger and Prince 1975) using F_o generated from the observed F_o^2 with the BAYES program (Blessing 1987), ionic scattering factors, and bulk compositional constraints. As is common practice, it was assumed that $^{[IV]}$Al and Si were at the tetrahedral site; Ti was confined to the M1 site; and Ca and Na were ordered at the M2 site. Mg and Mn were partitioned between the two octahedral sites M1 and M2, according to their concentrations (for details on the procedure of site occupancy determinations see Stimpfl et al. 1999). The results of the structural refinements are reported in Table 2 (interatomic distances) and in Table 4 (site occupancies, atomic coordinates, and thermal parameters). Partial molar fractions computed from site occupancies for each experiment are summarized in Table 5a, which includes some statistics from the structural refinement.

The X-ray intensity data for the untreated DP1 sample were also refined without chemical constraints for comparison with the results of Petersen et al. (1984). In particular, a complete binary composition (Mn-Mg) was assumed for DP1 and two scattering curves were refined by the RFINE90 program with the only constraint being that f(Mn) + f(Mg) = 1 (f = scattering curve) at both M1 and M2 sites. Results from this refinement are in Table 5b.

RESULTS

The untreated sample

Results from the structural refinement obtained for the untreated DP1 sample compare well with the data of Petersen et al.

TABLE 3. Measured (l) and adjusted (adj) compositions of the donpeacorite sample (DP1) used for the annealing experiments

Sample	DP1 (l)		DP1 (adj)
Si	1.9895	(50)	1.9969
Al	0.0073	(40)	0.0030
Ti	0.0005	(10)	0.0015
Mg	1.4379	(70)	1.4325
Fe	0.0000		0.0000
Mn	0.5446	(50)	0.5415
Ca	0.0250	(20)	0.0245
Na	0.0007	(10)	0.0000
Total	4.006		4.000
Charge	11.998		12.000
Al(T)*	0.007		0.003
Al(M)*	0.000		0.000
d[chr(M)]†	0.000		0.003
d(M-T) ‡	−0.007		0.000
M-cations	2.009		2.000
XMn§	0.275		0.274

Note: Standard deviations from the mean are given in parentheses.
*Al(T): Al at the T site; Al (M): Al at the M site.
† d[chr(M)]: excess positive charge at the M site due to the substitution for 2+ cations.
‡ d(M-T): difference between the charge excess at the M site and the charge deficiency at the T site.
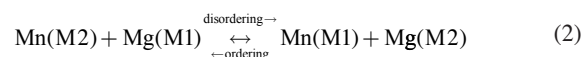§ XMn = Mn / (Mn + Mg).

(1984) determined for another donpeacorite single crystal from the same locality. Agreement between the two data sets is very good for the interatomic distances and the atomic coordinates but there is a discrepancy with respect to the site occupancies at the M1 and M2 sites. While Petersen et al. (1984) report that all Mn is fully ordered at M2, a small amount of Mn was observed at M1 for DP1 (Table 5b). This result is also valid when the structural refinement is carried out taking into account the full composition of the system (refinement with chemical constraints - Table 5a). A possible explanation for this discrepancy might rest in the small number of X-ray reflections used by Petersen et al. (1984). In their work the data collection was carried out to 55° in 2θ and only 801 independent reflections were available for the structure refinement; for this work, the data collection covered up to ~80° in 2θ and a total of ~2500 reflections was used to recover the geometry and the site occupancy (Table 5b). Even though a small amount of Mn is present at the M1 site in the untreated sample (Table 5a and 5b), Mn overwhelmingly orders at M2.

Fractionation experiments

Site occupancy data were used to compute the intracrystalline distribution coefficient $k_{\mathrm{D(Mn-Mg)}}$ which for the exchange reaction in donpeacorite is defined as:

$$k_{\mathrm{D(Mn-Mg)}} = \frac{X\mathrm{Mn(M1)}X\mathrm{Mg(M2)}}{X\mathrm{Mn(M2)}X\mathrm{Mg(M1)}} \qquad (1)$$

according to the homogeneous exchange reaction:

$$\mathrm{Mn(M2)} + \mathrm{Mg(M1)} \underset{\leftarrow \mathrm{ordering}}{\overset{\mathrm{disordering} \rightarrow}{\leftrightarrow}} \mathrm{Mn(M1)} + \mathrm{Mg(M2)} \qquad (2)$$

where XMn(M2) is the partial molar fraction of Mn in M2 defined as XMn(M2) = Mn(M2) / [Mn(M2) + Mg(M2)], and similarly for the other terms.

A weighted linear regression of $\ln k_{\mathrm{D(Mn-Mg)}}$ vs. $1/T$(K) (Table 5a) in the form $\ln k_\mathrm{D} = -\Delta H°/RT + \Delta S°/R$ yields the following result:

$$\ln k_\mathrm{D} = -\frac{2752(\pm 158)}{T(\mathrm{K})} - 0.348(\pm 0.137) \ (R^2 = 99\%) \qquad (3)$$

where the $\ln k_\mathrm{D}$ values were weighted by $1/[\sigma(\ln k_\mathrm{D})]^2$ where σ represents the estimated standard deviation.

DISCUSSION

Preference of Mn and Fe²⁺ for the M2 site

The data in Table 5a support the observation of Hawthorne and Ito (1978) that Mn fractionates over the octahedral sites in orthopyroxene similarly to Fe^{2+}: both order to M2, with the extent of ordering decreasing with temperature.

To determine whether Mn and Fe^{2+} show the same fractionation behavior, Equation 3 was compared with a calibration determined for Fe-Mg orthopyroxene with compositions XFe = 0.19–0.75 (Stimpfl et al. 1999). If Fe and Mn respond to a change in temperature to the same degree, then there should be no statistically significant difference between the two calibrations. Figure 1 shows a comparison of the $k_{\mathrm{D(Mn-Mg)}}$ values determined in this study with $k_{\mathrm{D*(Fe-Mg)}}$ (where * means that Mn was partitioned

TABLE 4. Atomic coordinates for DP1 and site occupancies for the untreated and heat treated samples.

Heating treatment	Untreated	980 °C DIS	900 °C DIS	904 °C ORD	856 °C ORD	806 °C ORD
M1	$Mg_{.9882}Mn_{.0103}Ti_{.0015}$	$Mg_{.9300}Mn_{.0685}Ti_{.0015}$	$Mg_{.9362}Mn_{.0623}Ti_{.0015}$	$Mg_{.9371}Mn_{.0614}Ti_{.0015}$	$Mg_{.9419}Mn_{.0566}Ti_{.0015}$	$Mg_{.9458}Mn_{.0527}Ti_{.0015}$
x	0.37530 (2)	0.37541 (2)	0.37542 (2)	0.37541 (2)	0.37537 (2)	0.37537 (2)
y	0.65408 (4)	0.65383 (4)	0.65387 (5)	0.65387 (4)	0.65390 (5)	0.65388 (4)
z	0.87230 (8)	0.87209 (6)	0.87215 (7)	0.87216 (8)	0.87221 (8)	0.87211 (8)
B_{iso}	0.5218	0.4555	0.5294	0.453	0.4741	0.4982
M2	$Mg_{.4443}Mn_{.5312}Ca_{.0245}$	$Mg_{.5025}Mn_{.4730}Ca_{.0245}$	$Mg_{.4963}Mn_{.4792}Ca_{.0245}$	$Mg_{.49545}Mn_{.4480}Ca_{.0245}$	$Mg_{.4906}Mn_{.4849}Ca_{.0245}$	$Mg_{.4867}Mn_{.4888}Ca_{.0245}$
x	0.37762 (1)	0.37747 (1)	0.37743 (1)	0.37742 (1)	0.37747 (1)	0.37742 (1)
y	0.47989 (3)	0.48056 (3)	0.48061 (3)	0.48057 (3)	0.48048 (3)	0.48038 (3)
z	0.36852 (5)	0.36819 (4)	0.36829 (5)	0.36833 (5)	0.36825 (5)	0.36831 (5)
B_{iso}	0.7519	0.6798	0.7595	0.6935	0.7159	0.7196
SiA						
x	0.27102 (2)	0.27114 (2)	0.27114 (1)	0.27114 (1)	0.27113 (2)	0.27112 (2)
y	0.34120 (3)	0.34110 (3)	0.34111 (4)	0.34107 (3)	0.34110 (4)	0.34111 (3)
z	0.04763 (6)	0.04843 (5)	0.04843 (6)	0.04833 (7)	0.04828 (6)	0.04829 (6)
B_{iso}	0.4224	0.3508	0.4242	0.3639	0.3798	0.3896
SiB	$Si_{.9969}Al_{.0031}$	$Si_{.9969}Al_{.0031}$	$Si_{.9969}Al_{.0031}$	$Si_{.9969}Al_{.0031}$	$Si_{.9969}Al_{.0031}$	$Si_{.9969}Al_{.0031}$
x	0.47494 (2)	0.47477 (1)	0.47481 (1)	0.47480 (1)	0.47480 (2)	0.47480 (2)
y	0.33794 (3)	0.33774 (3)	0.33777 (4)	0.33776 (3)	0.33782 (4)	0.33782 (3)
z	0.79557 (6)	0.79486 (5)	0.79492 (6)	0.79497 (7)	0.79504 (7)	0.79509 (7)
B_{iso}	0.4331	0.3591	0.4258	0.3565	0.3843	0.3921
O1A						
x	0.18322 (4)	0.18343 (4)	0.18342 (4)	0.18343(4)	0.18336 (4)	0.18333 (5)
y	0.33835 (9)	0.33862 (7)	0.33867(10)	0.33864(9)	0.33845(10)	0.33863 (9)

Note: Standard deviations are given in parentheses. Abbreviations as in Table 1. Site occupancies are equal to 1 unless stated differently

as Fe) in orthopyroxene of composition XFe = 0.19–0.75, as determined by Stimpfl et al. (1999).

These comparative data show that although Mn and Fe^{2+} prefer the M2 site, relative to Mg, Mn has a significantly stronger M2 site preference than Fe. A similar conclusion was reached by Ghose et al. (1975), who suggested on crystal-chemical grounds the following M2 site preference $Mn^{2+} > Zn^{2+} > Fe^{2+} > Co^{2+} >> Mg > Ni^{2+}$ for (Mg, M^{2+}) orthopyroxene.

The partitioning of transition metals among different crystallographic sites depends on several factors including crystal field stabilization energy (CFSE); degree of covalency of the M-O bond; structural geometry of the site (size, deviation from a regular polyhedron); and valence and size of the ion (Schwarcz 1967; Langer et al. 1999). The different preference of Mn and Fe^{2+} for the M2 site cannot be explained by CFSE or by the covalent character of the M2-O bonds (O'Nions and Smith 1973). In fact, due to its electronic configuration (d5) Mn undergoes no crystal field stabilization (Schwarcz 1967; Burns 1993), and Fe^{2+} displays a higher degree of covalency than what is expected for Mn^{2+}. These energetic effects, therefore, seem not to be responsible for the observed trend. On the other hand, pure stereochemical arguments can explain the experimental results. The ionic radius of Mn is slightly larger than that of Fe^{2+} (0.83 and 0.78 Å, respectively) but is much larger than that of Mg (0.73 Å) in octahedral coordination (Shannon and Prewitt 1969). The greater preference of Mn for the M2 site is probably a sole consequence of the difference in ionic radii between Mn and Mg. Comparison of the volumes of the octahedral sites of DP1 (untreated) with those of an orthopyroxene (GRO) whose XFe ~ XMn in DP1 exemplifies this point. The M1 site volume for both DP1 and GRO are quite similar: 11.94 and 11.92 Å³ respectively; on the other hand, the volumes for the M2 site are very different: 13.35 and 12.95 Å³ for DP1 and GRO respectively, with a ratio equal to 1.03. For an equivalent composition, the M2 site in DP1 is larger than the M2 site in GRO. The greater contrast in size between the Mn/Mg pair compared to the Fe/Mg pair dominates
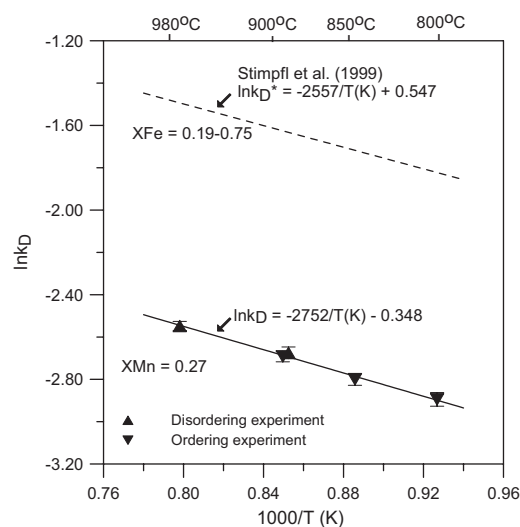
FIGURE 1. Comparison of Mn and Fe partitioning behavior in donpeacorite and Fe-Mg orthopyroxene. Intracrystalline distribution coefficients (k_D) for the donpeacorite sample DP1 as determined in this study (upward triangles: disordering experiments; downward triangles: ordering experiments) and the corresponding least-squares fit (solid line) are shown. The dashed line is for Fe-Mg orthopyroxenes of composition XFe = 0.19–0.75 (Stimpfl et al. 1999).

the site preference for Mn; however, its size is still small enough to allow for some disordering at the M1 site.

Comparison between $\ln k_{D*}$ and $\ln k_D$ calibrations for Fe,Mg orthopyroxene

Stimpfl et al. (1999) determined the equilibrium site fractionation for four natural orthopyroxene crystals with compositions ranging from XFe = 0.14–0.50 at temperatures between 1000–550 °C using X-ray diffraction. The k_{D*} values from their study were then combined with data carefully selected from the literature to

TABLE 4.—*Continued*

Heating treatment	Untreated	980 °C DIS	900 °C DIS	904 °C ORD	856 °C ORD	806 °C ORD
z	0.04092(16)	0.04032(17)	0.04050(15)	0.04059(18)	0.04042(17)	0.04025(17)
B_{iso}	0.4471	0.4475	0.4475	0.4479	0.4474	0.4468
O2A						
x	0.30974 (4)	0.30988 (4)	0.30982(4)	0.30987 (4)	0.30983 (4)	0.30981 (5)
y	0.50196 (9)	0.50158 (8)	0.50160(10)	0.50165 (9)	0.50166(10)	0.50159 (9)
z	0.04548(16)	0.04639(15)	0.04651(16)	0.04640(18)	0.04622(18)	0.04607(17)
B_{iso}	0.6249	0.5699	0.6283	0.5762	0.596	0.6084
O3A						
x	0.30222 (4)	0.30235 (4)	0.30228 (4)	0.30231 (4)	0.30223 (4)	0.30224 (5)
y	0.22933(10)	0.22899 (8)	0.22905(11)	0.22897(10)	0.22917(11)	0.22911(10)
z	0.82166(16)	0.82249(14)	0.82286(16)	0.82264(17)	0.82235(17)	0.82245(17)
B_{iso}	0.7016	0.6058	0.6873	0.6158	0.6328	0.6544
O1B						
x	0.56305 (4)	0.56286 (4)	0.56293 (4)	0.56294 (4)	0.56299(4)	0.56299 (5)
y	0.33850 (9)	0.33919 (8)	0.33911(10)	0.33916 (9)	0.33903(10)	0.33892 (9)
z	0.79752(16)	0.79654(14)	0.79670(15)	0.79617(18)	0.79668(17)	0.79688(17)
B_{iso}	0.5493	0.5044	0.5532	0.5025	0.5212	0.5149
O2B						
x	0.43529 (5)	0.43490 (4)	0.43493 (4)	0.43494 (4)	0.43495 (5)	0.43501 (6)
y	0.48760 (9)	0.48658 (8)	0.48675(11)	0.48667 (9)	0.48674(11)	0.48701 (9)
z	0.70173(17)	0.69994(15)	0.70004(17)	0.70069(19)	0.70045(18)	0.70056 (9)
B_{iso}	0.7595	0.6916	0.7622	0.7356	0.7196	0.7434
O3B						
x	0.44758 (4)	0.44776 (4)	0.44773 (4)	0.44781 (4)	0.44769 (4)	0.44774 (5)
y	0.20399(10)	0.20331 (9)	0.20355(11)	0.20351(10)	0.20372(12)	0.20373(10)
z	0.59139(16)	0.59138(14)	0.59141(15)	0.59125(17)	0.59169(17)	0.59118(17)
B_{iso}	0.7016	0.5936	0.7044	0.6256	0.6291	0.6875

TABLE 5A. Partial molar fraction for M1 and M2, $-\ln k_D$, and statistics for the structural refinements of DP1 for the relevant heating treatments

Heating treatment (annealing time)	*$XMn(M1)$	*$XMn(M2)$	$-\ln k_D$	†GOF	$R(Fo)w\%$
Untreated	0.0104 (18)	0.5455 (18)	4.7437 (1723)	1.05	2.1
980 °C DIS (120 h)	0.0686 (15)	0.4849 (15)	2.5480 (217)	1.05	2.7
900 °C DIS (72 h)	0.0624 (17)	0.4912 (17)	2.6746 (276)	1.06	2.4
904 °C ORD (72 h)	0.0616 (16)	0.4921 (16)	2.6919 (251)	1.04	2.9
856 °C ORD (456 h)	0.0567 (16)	0.4971 (16)	2.8000 (280)	1.05	2.7
806 °C ORD (720 h)	0.0527 (18)	0.4989 (18)	2.8846 (322)	1.04	2.8

Notes: The time in hours (hrs) indicates the total annealing time for each experiment. Standard deviations are given in parenthesis.
* $XMn(M1) = Mn(M1) / [Mn(M1) + Mg(M1)]$, and similarly for M2.
† GOF = goodness of fit.

develop an expression for k_{D*} as a function of temperature and composition. The calibration of Stimpfl et al. (1999) has been used in several studies to recover the cooling history of host rocks and also to determine the kinetics of the O/D reaction in orthopyroxene (Ganguly and Stimpfl 2000; Goodrich et al. 2001; Zema et al. 2003).

To evaluate errors introduced in the calibration by using Fe* (i.e., Fe^{2+} + Mn) as a partitioning species, we used the intensity data collected by Stimpfl et al. (1999) to refine the site occupancies for the relevant annealing experiment by partitioning only Fe. The structural refinement procedure is described in detail in Stimpfl et al. (1999); the only difference between the two procedures is that in this work Fe was the only fractionating species. However, modeling shows that for Mn concentrations found in the samples used by Stimpfl et al. (1999) - SJN $Dp_{0.9}$, ST77 $Dp_{0.8}$, and HO28 $Dp_{0.7}$ - if ideal behavior is assumed, Equation 3 predicts a small amount of Mn at M1 for temperatures higher than 900 °C, while for lower temperatures virtually all Mn is ordered at M2. In particular, $XMn(M1) > 0.001$ for temperatures above 900 °C, and $XMn(M1) < 0.001$ for temperatures below 900 °C. To account for this small fractionation at high temperatures we computed,

via Equation 3, the amount of Mn to be assigned a priori to M1 and M2 for Stimpfl et al.'s (1999) three higher-temperature runs (ST77 900 °C DIS, ST77 900 °C ORD, and ST77 1000 °C DIS) while for the lower temperature experiments Mn was not fractionated and was kept completely ordered at M2. Failure to take into account the fractionation of Mn at high temperature for the low-Fe sample translates to more disordered k_D's.

The results from these structural refinements are listed in Table 6, together with the relevant $\ln k_{D(Fe-Mg)}$ and $\ln k_{D*}$ values [$k_{D*} = (Fe*/Mg)^{M1}/(Fe*/Mg)^{M2}$] published in Stimpfl et al. (1999) for the same experiment. The difference between $\ln k_{D(Fe-Mg)}$ and $\ln k_{D*}$ is mostly contained within the standard deviation of $\ln k_D$ which indicates that different partitioning methods (Fe vs. Fe*) only marginally affect the k_D values. However, ordering of Mn at M2 systematically generates a more disordered configuration (i.e., $\ln k_{D(Fe-Mg)} > \ln k_{D*}$) with the greater difference for the low-Fe orthopyroxene.

Linear regression of $\ln k_{D(Fe-Mg)}$ vs. $1/T(K)$ for the data listed in Table 6 yields for the Fe-rich sample HO28:

$$\ln k_D = -\frac{2708(\pm 58)}{T(K)} - 0.695(\pm 0.058) \quad (R^2 = 100\%) \tag{4}$$

Equation 4 excludes the 550 °C ORD data, which did not reach equilibrium within the time frame of the experiment (see Stimpfl et al. 1999). For the low-Fe samples SJN and ST77 the implied regression yields:

$$\ln k_D = -\frac{2984(\pm 69)}{T(K)} - 0.747(\pm 0.078) \quad (R^2 = 99\%). \tag{5}$$

For HO28 (Fs_{50}), Equation 4 and the corresponding regression of Stimpfl et al. (1999) are virtually indistinguishable (Fig. 2). For the low-Fe pyroxenes (SJN - Fs_{14}; ST77 - Fs_{16}), the high-temperature range of Equation 5 defines a slightly more

TABLE 5B. Site occupancies for the untreated DP1 sample determined without bulk chemical constraints, compared to the results of Petersen et al. (1984)

Sample	*Mn(M1)	* Mn(M2)	† –lnk_D	2θ	‡No. Ind. Reflex.	R(Fo)sym%	R(Fo)%
DP1	0.0159 (27)	0.5431 (27)	4.2982(1692)	80	2449	1.91	2.6
Petersen et al. (1984)	–0.0200 (100)	0.5300(100)	n.a.	55	801	–	5.0

Notes: The table also lists some parameters relevant to the data collection and structural refinement. Standard deviations are given in parenthesis.
* Site occupancies determined without chemical constraints and assuming binary composition.
† "Crystallographic" k_D does not take into account the full chemical composition.
‡ No. ind. reflex. = Number of independent reflections.

TABLE 6. Conditions of annealing experiments and results of site occupancy refinement obtained by partitioning only Fe

Sample	- Heating treatment	XFeM1		XFeM2		–lnk_D		* –lnk_{D^*}	Δ(lnk_D's)
SJN (Fs$_{14}$Dp$_{0.9}$)	–700 °C ORD	0.0319	(12)	0.2535	(12)	2.3321	(391)	2.3784	–0.0463
SNJ	–750 °C DIS	0.0360	(17)	0.2492	(17)	2.1857	(498)	2.2089	–0.0232
SNJ	–750 °C ORD	0.0362	(8)	0.2492	(8)	2.1794	(239)	2.2148	–0.0354
SNJ	–800 °C DIS	0.0411	(9)	0.2441	(9)	2.0191	(218)	2.0724	–0.0533
ST77 (Fs$_{16}$Dp$_{0.8}$)	–700 °C DIS	0.0352	(10)	0.2779	(10)	2.3562	(285)	2.3179	0.0383
ST77	–700 °C ORD	0.0353	(9)	0.2777	(9)	2.3513	(252)	2.3702	–0.0189
ST77	–800 °C DIS	0.0474	(10)	0.2654	(10)	1.9827	(211)	2.0096	–0.0269
ST77	–800 °C ORD	0.0469	(10)	0.2660	(10)	1.9966	(214)	2.0229	–0.0263
ST77†	–900 °C DIS	0.0545	(9)	0.2580	(9)	1.7972	(175)	1.8180	–0.0208
ST77†	–900 °C ORD	0.0543	(10)	0.2582	(10)	1.8019	(564)	1.8257	–0.0238
ST77†	–1000 °C DIS	0.0628	(10)	0.2496	(10)	1.6018	(159)	1.6604	–0.0586
HO28 (Fs$_{50}$Dp$_{0.7}$)	–550 °C DIS	0.2272	(10)	0.7986	(10)	2.6017	(81)	2.6133	–0.0116
HO28	–550 °C ORD	0.2330	(10)	0.7926	(10)	2.5323	(75)	2.5411	–0.0088
HO28	–650 °C DIS	0.2581	(10)	0.7667	(10)	2.2456	(66)	2.2545	–0.0089
HO28	–650 °C ORD	0.2598	(10)	0.7650	(10)	2.2273	(65)	2.2393	–0.0120
HO28	–750 °C DIS	0.2851	(10)	0.7389	(10)	1.9597	(64)	1.9743	–0.0146
HO28‡	–750 °C ORD	0.2862	(11)	0.7378	(11)	1.9485	(63)	1.9571	–0.0086
HO28	–850 °C DIS	0.3098	(11)	0.7134	(11)	1.7131	(61)	1.7308	–0.0177

Notes: The intensity data for the annealing experiments were collected by Stimpfl et al. (1999). Values of lnk_{D^*} (k_{D^*} = (XFe*/XMg)^{M1}/(XFe*/XMg)^{M2}) are taken from Stimpfl et al. (1999) for the relevant annealing experiments. Δ(lnk_D) = (lnk_{D^*} – lnk_D); the standard deviations are in parenthesis.
* Equilibrium values as in Stimpfl et a. (1999).
† For these temperatures Mn was partitioned a priori at M1 and M2 according to Equation 3.
‡ The lnk_{D^*} for this isotherm is misreported in Stimpfl et al. (1999); here we report the correct value.

disordered configuration compared to the calibration obtained by Fe* partitioning (Stimpfl et al. 1999).

As expected from the low total concentration of Mn, the various partitioning procedures have only marginal effects on k_D. However, the difference in k_D is mainly reflected in the value of XFe(M2) and is more prominent in low-Fe orthopyroxene than in high-Fe orthopyroxene. Comparison of an annealing experiment for a high-Fe orthopyroxene with that for a low-Fe orthopyroxene exemplifies this point. For the sample HO (Fs$_{50}$), comparison of the data at 850 °C obtained through the two partitioning procedures shows that the percentage difference in site occupancy in M2 amounts to less than 0.3%. On the other hand, for sample SJN (Fs$_{16}$), at 800 °C partitioning of only Fe over M1 and M2 yields XFe(M1) = 0.0411, XFe(M2) = 0.2441 (Table 6), whereas Fe* partitioning yields XFe*(M1) = 0.0420, XFe*(M2) = 0.2583 (Stimpfl et al. 1999). This translates to a difference in XFe(M2) of ~ 6%. However, as the Mn content in Fe-Mg orthopyroxene increases, the difference in site occupancies (and k_D's) between the two partitioning methods would strongly affect more Fe-rich samples as well. In particular, as the Fe/Mn ratio decreases, the samples will become more sensitive to the type of partitioning method used, i.e., Fe* vs. Fe.

Implications for cooling histories of natural samples

The overestimation of the degree of ordering generated by partitioning Fe* instead of Fe will have consequences for the determination of cooling rates from observed site occupancies.

To quantify this effect, cooling rates for an intermediate-Fe orthopyroxene (GRO1 Fs$_{23}$- Stimpfl and Ganguly 2002) and a low-Fe sample (SJN24 Fs$_{14}$- Ganguly and Stimpfl 2000) were recomputed using the kinetic data of Ganguly and Stimpfl (2000). New site occupancies were obtained by refining the observed intensity data of GRO1 and SJN24 keeping Mn ordered completely at M2 according to the findings of this study (see Ganguly and Stimpfl 2000 for the procedures used to determine cooling rates from the state of order in orthopyroxene).

The partitioning procedure had dramatic effects on the calculated cooling rates depending on the relative proportion of Fe and Mn (Table 7). For the intermediate-Fe sample, the small effect of the partitioning methods on k_D and XFe(M2) translates to no change in the cooling rate. In marked contrast, however, for the low-Fe sample the calculated cooling rate increases by 350% when Fe is partitioned independently from Mn (similar results were obtained for sample ST77 with Fs$_{16}$). This conclusion was also reached by Schlenz et al. (2001) who pointed out that the cooling rates determined for low-Fe compositions are more sensitive to error in the microprobe analyses: using Fe* as the partitioning species is, in a way, equivalent to an overestimation of total Fe in the system.

Partitioning Mn as Fe will therefore affect the cooling rates based on the observed ordering state in natural samples and will bias the interpretation of the *T*-t evolution of the parent rock toward slower cooling. This in turn will affect exhumation rates or depth of burial that are recovered from the cooling rates. For this

TABLE 7. Comparison of effect of partitioning methods (Fe* vs. Fe) on cooling rates computed for orthopyroxenes of two different compositions

Sample	SJN24 ($Fs_{14}Dp_{0.9}$)		GRO1($Fs_{23}Dp_{0.8}$)	
Part. meth.	* Fe*	Fe only	† Fe*	Fe only
°C/m.y.	201	696	135	134

Notes: The composition of each sample is reported in parenthesis next to the sample's label. Part. meth. = Partitioning method.
* Data from Ganguly and Stimpfl (2000).
† Data from Stimpfl and Ganguly (2002).
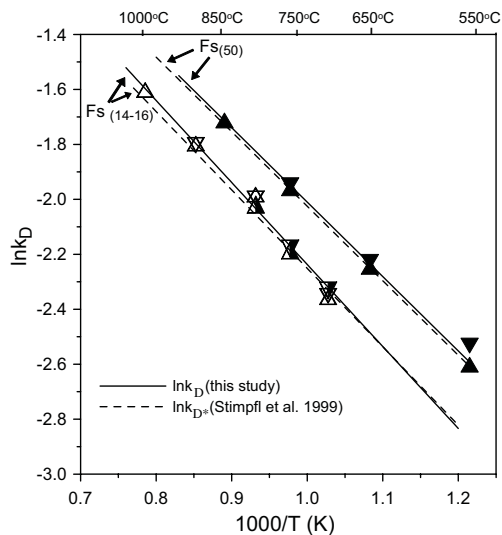
FIGURE 2. Comparison of $\ln k_D$ (solid lines) and $\ln k_{D*}$ (dashed lines) vs. $1/T(K)$ for orthopyroxenes of composition Fs_{50} (upper lines) and Fs_{14-16} (lower lines). The triangles represent the values of k_D determined in this work by partitioning only Fe, with the exception of experiments conducted at temperatures higher than or equal to 900 °C. For these data Mn was assigned a priori to M1 and M2 according to Equation 3 (see text for more details). The solid lines show the least squares regression through the data, while the dashed line represent calibrations taken for the same composition from Stimpfl et al. (1999). Filled triangles: sample HO28 (Fs_{50}); empty triangles: sample ST77 (Fs_{16}); half filled triangles: sample SJN (Fs_{14}) (orientation of the symbols as in Fig. 1).

reason we recommend avoiding the practice of partitioning Fe and Mn as a single species (Fe*). This is particularly important when the Fs component of the orthopyroxene is small (Fs < 0.16) as seen in the example give in the previous section.

REFERENCES CITED

Anovitz, L.M., Essene, E.J., and Dunham, W.R. (1988) Order-disorder experiments on orthopyroxenes: Implication for the orthopyroxene geospeedometer. American Mineralogist, 73, 1060–1073.
Besancon, J.R. (1981) Rate of cation disordering in orthopyroxenes. American Mineralogist, 66, 965–973.
Blessing, R.H. (1987) Data reduction and error analysis for accurate single crystal diffraction intensities. Crystallographic Reviews, 1, 3–58.
Bruker (1997a) SAINT Reference Manual Version 5. Madison, Wisconsin, U.S.A., Bruker AXS Inc.
——— (1997b) SMART Reference Manual Version 5. Madison, Wisconsin, U.S.A., Bruker AXS Inc.
Burns, R.G. (1993) Mineralogical applications of crystal field theory. Cambridge University Press, Cambridge
Dollase, W.A. and Newman, W.I. (1984) Statistically most probable stoichiometric formulae. American Mineralogist, 69, 553–556.
Domeneghetti, M.C., Molin, G., Stimpfl, M., and Tribaudino, M. (1995) Orthopyroxene from the Serra de Magè meteorite: Structure refinement and estimation of C2/c pyroxene contributions to apparent P*bca* diffraction violations. American Mineralogist, 80, 923–929.
Finger, L.W. and Prince, E. (1975) A system of FORTRAN IV computer programs for crystal structural computations. NBS Tech Notes, 854.
Ganguly, J. and Domeneghetti, M.C. (1996) Cation ordering of orthopyroxene from the Skaegaard intrusion: implication for the subsolidus cooling rates and permeabilities. Contributions to Mineralogy and Petrology, 122, 359–367.
Ganguly, J. and Stimpfl, M. (2000) Cation ordering in orthopyroxenes from two stony iron meteorites: Implications for cooling rates and metal-silicate mixing. Geochimica et Cosmochimica Acta, 64/7, 1291–1297.
Ganguly, J. and Tazzoli, V. (1994) Fe^{2+}-Mg interdiffusion in orthopyroxene: Retrieval from the data on intracrystalline exchange reaction. American Mineralogist, 79, 930–937.
Ganguly, J., Yang, H., and Ghose, S. (1994) Thermal history of mesosiderites: Quantitative constraints from compositional zoning and Fe-Mg ordering in orthopyroxenes. Geochimica et Cosmochimica Acta, 58, 2711–2723.
Ghose, S., Wan, C., and Okamura, F.P. (1975) Site preference and crystal chemistry of transition metal ions in pyroxene and olivine. Acta Crystallographica, A31, 576.
Goodrich, C.A., Fioretti, A.M., Tribaudino, M., and Molin, G. (2001) Primary trapped melt inclusions in olivine in the olivine-augite-orthopyroxene ureilite Hughes 009. Geochimica et Cosmochimica Acta, 65, 621–652.
Hawthorne, F.C. and Ito, J. (1978) Refinement of the crystal structures of $(Mg_{0.776}Co_{0.224})SiO_3$ and $(Mg_{0.925}Mn_{0.075})SiO_3$. Acta Crystallographica, B34, 891–893.
Heinemann, R., Kroll, H., Langenhorst, F., and Lueder, T. (2000) Time and temperature variation of the intracrystalline Fe^{2+}, Mg fractionation in Johnstown meteoritic orthopyroxene. European Journal of Mineralogy, 12, 163–176.
Kroll, H., Lueder, T., Schlenz, H., Kirfel, A., and Vad, T. (1997) The Fe^{2+}, Mg distribution in orthopyroxene: a critical assessment of its potential as a geospeedometer. European Journal of Mineralogy, 9, 705–733.
Langer, K. and Khomenko, V.M. (1999) The influence of crystal field stabilization energy on Fe^{2+} partitioning in paragenetic minerals. Contributions to Mineralogy and Petrology, 137, 220–231.
Molin, G.M., Saxena, S.K., and Brizi, E. (1991) Iron-magnesium order-disorder in an opx crystal from the Johnstown meteorite. Earth and Planetary Science Letters, 105, 260–265.
O'Nions, R.K. and Smith, D.G.W. (1973) Bonding in silicates: an assessment of bonding in orthopyroxene. Geochimica et Cosmochimica Acta, 37, 249–257.
Petersen, E.U., Anovitz, L.M., and Essene, E.J. (1984) Donpeacorite, $(Mn,Mg)MgSi_2O_6$, a new orthopyroxene and its proposed phase relations in the system $MnSiO_3-MgSiO_3-FeSiO_3$. American Mineralogist, 69, 472–480.
Schlenz, H., Kroll, H., and Phillips, M.W. (2001) Isothermal annealing and continuous cooling experiments on synthetic orthopyroxenes: temperature and time evolution of the Fe, Mg distribution. European Journal of Mineralogy, 13, 715–726.
Schwarcz, H.P. (1967) The effect of crystal field stabilization on the distribution of transition metals between metamorphic minerals. Geochimica et Cosmochimica Acta, 31, 503–517.
Shannon, R.D. and Prewitt, C.T. (1969) Effective atomic radii in oxides and fluorides. Acta Crystallographica, Section B, 25, 925–946.
Sheldrick, G.M. (1996) SADABS. Siemens Area Detector Absorption Software. Germany, University of Göttingen.
Stimpfl, M. and Ganguly, J. (2002) Thermal history of the unbrecciated diogenite GRO (Grosvenor Mountains) 95555: constraints from inter-and intracrystalline Fe-Mg exchange reaction. Lunar and Planetary Science Proceedings, XXXIII., no. 1966.
Stimpfl, M., Ganguly, J., and Molin, G. (1999) Fe^{2+}-Mg order-disorder in orthopyroxene: Equilibrium fractionation between the octahedral sites and thermodynamic analysis. Contributions to Mineralogy and Petrology, 136, 297–309.
Zema, M., Domeneghetti, M.C., Molin, G.M., and Tazzoli, V. (1997) Cooling rates of diogenites: a study of Fe^{+2}-Mg ordering in orthopyroxene by single-crystal X-ray diffraction. Meteoritics and Planetary Science, 32, 855–862.
Zema, M., Tarantino, S.C., Domeneghetti, M.C., and Tazzoli, V. (2003) Ca in orthopyroxene: structural variations and kinetics of the disordering process. European Journal of Mineralogy, 15, 373–380.